

Effects of Low-Concentration Graphene Oxide Quantum Dots on Improving the Proliferation and Differentiation Ability of Bone Marrow Mesenchymal Stem Cells through the Wnt/ β -Catenin Signaling Pathway

Duoling Xu,[†] Chao Wang,[†] Jie Wu, Yuanxiang Fu, Shujun Li, Wentao Hou, Ling Lin, Pei Li, Dongsheng Yu,^{*} and Wei Zhao^{*}



Cite This: *ACS Omega* 2022, 7, 13546–13556



Read Online

ACCESS |



Metrics & More

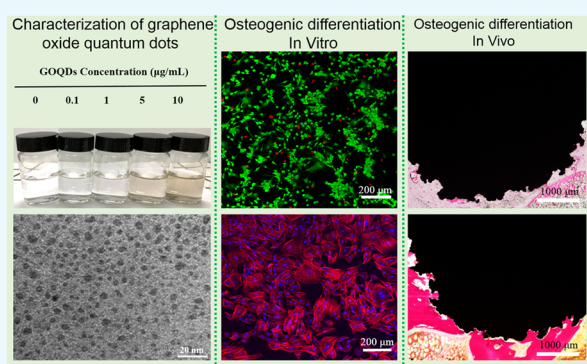


Article Recommendations



Supporting Information

ABSTRACT: Graphene oxide quantum dots (GOQDs) are considered to be a new method for regulating the proliferation and differentiation of bone marrow mesenchymal stem cells (BMSCs). However, there are few reports on such regulation with different concentrations of GOQDs, and the molecular mechanism has not been fully elucidated. The purposes of this study were, first, to explore the effects of GOQDs on the proliferation and differentiation of BMSCs *in vitro* and *in vivo*, and, second, to provide a theoretical basis for the repair of bone defects. Live/Dead staining, EdU staining, immunofluorescence staining, alkaline phosphatase (ALP), western blotting, and qT-PCR were used for detecting the proliferation and differentiation of BMSCs after coculture with GOQDs of different concentrations. Hematoxylin and eosin (HE) staining and Van Gieson (VG) staining were used to detect new bone regeneration *in vivo*. The results showed that low-concentration GOQDs (0.1 and 1 $\mu\text{g}/\text{mL}$) promoted the proliferation and differentiation of BMSCs. Compared with the 1 $\mu\text{g}/\text{mL}$ GOQD group, the 0.1 $\mu\text{g}/\text{mL}$ GOQD group had better ability to promote the proliferation and differentiation of BMSCs. HE and VG staining results showed the greatest proportion of new bone area on sandblasted, large-grit, and acid-etched (SLA)/GOQD scaffolds. Furthermore, the ratio of active β -catenin and the phosphorylation level of GSK-3 β (p-GSK-3 β) increased after BMSCs treatment with 0.1 $\mu\text{g}/\text{mL}$ GOQDs. Low concentrations of GOQDs improved the osteogenic differentiation ability of BMSCs by activating the Wnt/ β -catenin signaling pathway.



1. INTRODUCTION

Due to trauma, tumor, inflammation, and other factors, the incidence of oral and maxillofacial bone defects has increased sharply, with serious effects on the physical and mental health of affected patients.¹ Nanoregenerative medicine has become an important method for the repair of bone defects.^{2–4} Bone marrow mesenchymal stem cells (BMSCs) can differentiate into different cell phenotypes, including osteoblasts, chondrocytes, etc. BMSCs are commonly used seed cells for repairing bone defects in nanoregenerative medicine.^{5,6} In the microenvironment of bone defects, the proliferation and osteogenic differentiation of BMSCs are essential conditions for promoting bone repair.⁷

At present, graphene and its derivatives have shown broad prospective applications in the field of biology due to their excellent mechanical properties, electrical conductivity, and atomic structural stability.⁸ Graphene oxide nanosheets can inhibit *Staphylococcus aureus* and *Escherichia coli*, preventing the aggravation of wound infection.⁸ As a derivative of graphene,

graphene oxide (GO) has become one of the most promising carbonaceous materials for cancer therapy due to its versatile surface chemistry and easy functionalization.⁹ Graphene and its derivatives can bring the desired electrical stimulation to cellular osteogenic activity and bone formation and facilitate the adsorption of active substances.¹⁰ Graphene oxide quantum dots (GOQDs) are transformed from GO, with quantum size and boundary effects, and have not only the excellent properties of GO but also new characteristics, such as better solubility, low cytotoxicity, and excellent biocompatibility.^{11–13}

Received: December 6, 2021

Accepted: April 7, 2022

Published: April 18, 2022



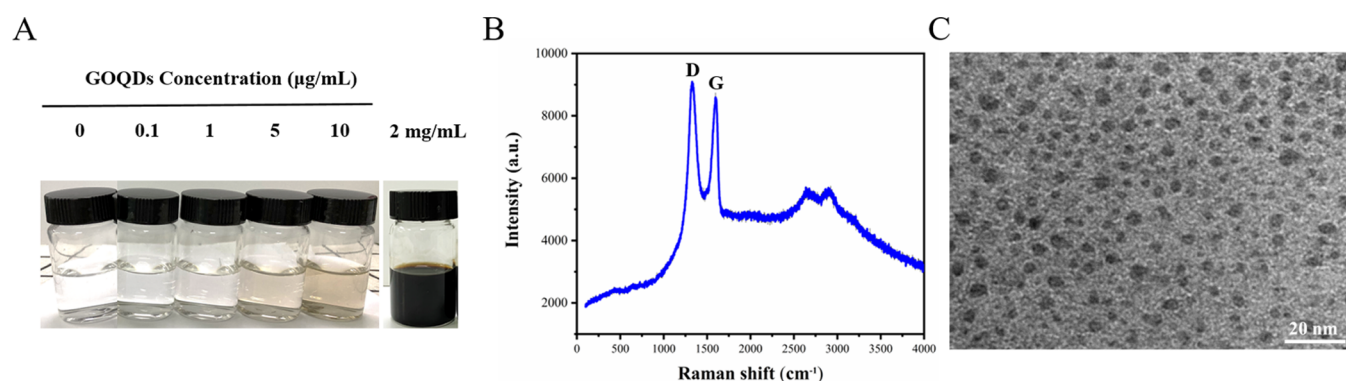


Figure 1. Characterization of GOQDs. (A) GOQDs suspension with concentrations of 0, 0.1, 1, 5, 10 $\mu\text{g/mL}$, and 2 mg/mL , respectively; (B) Raman spectra of GOQDs; and (C) TEM image of GOQDs.

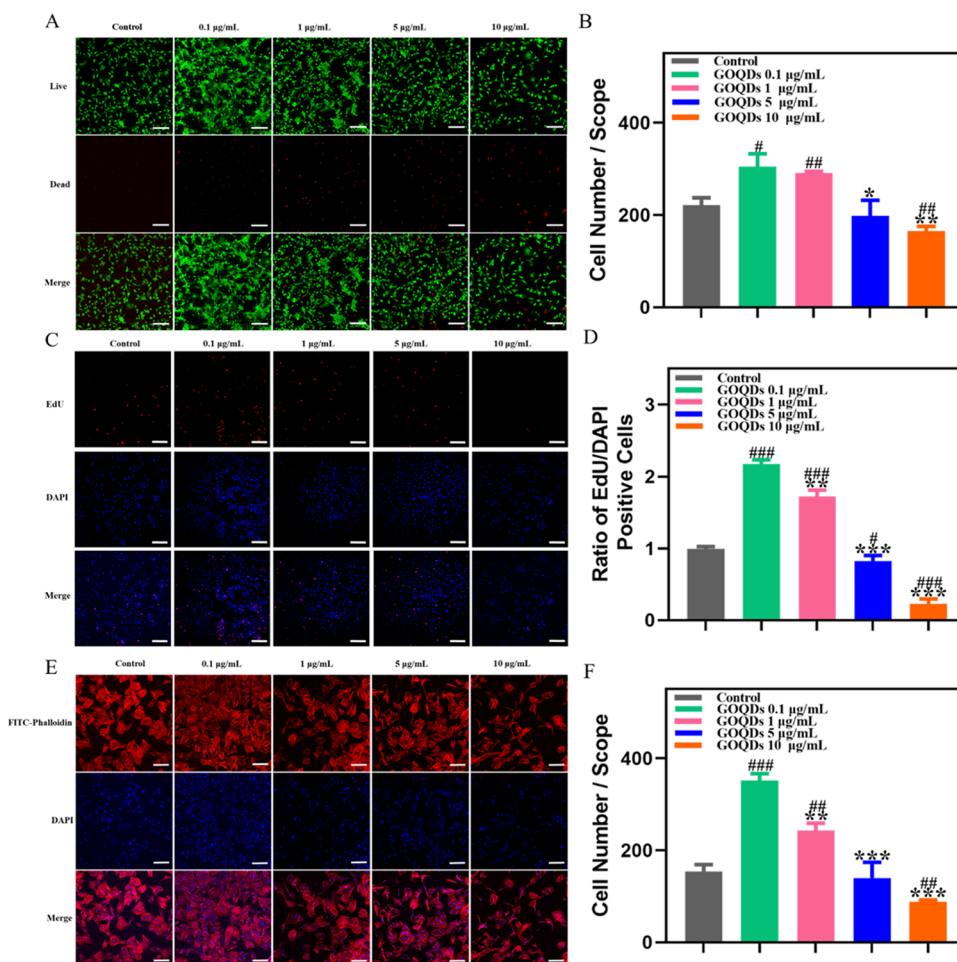


Figure 2. Effects of different concentrations of GOQDs on the viability, proliferation, and morphology of BMSCs. (A) Live/Dead staining image shows the cell viability of BMSCs cocultured with GOQDs at different concentrations for 3 days. Green indicates live cells and red indicates dead cells. (B) Number of living cells counted by means of ImageJ software, (C) EdU cell proliferation assay image showing the cell proliferation of BMSCs cocultured with GOQDs at different concentrations for 1 day, (D) ratio of EdU-positive cell, and (E) confocal laser images used to capture the cell morphology of BMSCs cocultured with different concentrations of GOQDs for 1 day after BMSCs were stained with phalloidin and DAPI. Red indicates actin filaments and blue indicates cell nuclei. (F) Number of cell nuclei was counted by means of ImageJ software. Scale bars: 200 μm ($*p < 0.05$, $**p < 0.01$, $***p < 0.001$, compared with 0.1 $\mu\text{g/mL}$ GOQDs, and $^{\#}p < 0.05$, $^{\#\#}p < 0.01$, and $^{\#\#\#}p < 0.001$, compared with control).

Numerous studies have reported that GO within a certain concentration range can promote the proliferation and differentiation of BMSCs.^{14–16} Liao et al. evaluated the effects of graphene nanosheets (GNs) with concentrations of 0, 1, 10, 30, 50, and 100 $\mu\text{g/mL}$ on the osteogenic differentiation of MSCs. These results demonstrated that when the GNs

concentrations were lower than 10 $\mu\text{g/mL}$, GNs improved the proliferation and osteogenic differentiation ability of MSCs.¹⁷ Qiu et al. studied the effects of GOQDs at concentrations of 0, 1, 10, and 100 $\mu\text{g/mL}$ on MSCs, and found that when the concentration of graphene was lower than 10 $\mu\text{g/mL}$, it was more conducive to osteoblast proliferation.¹⁸

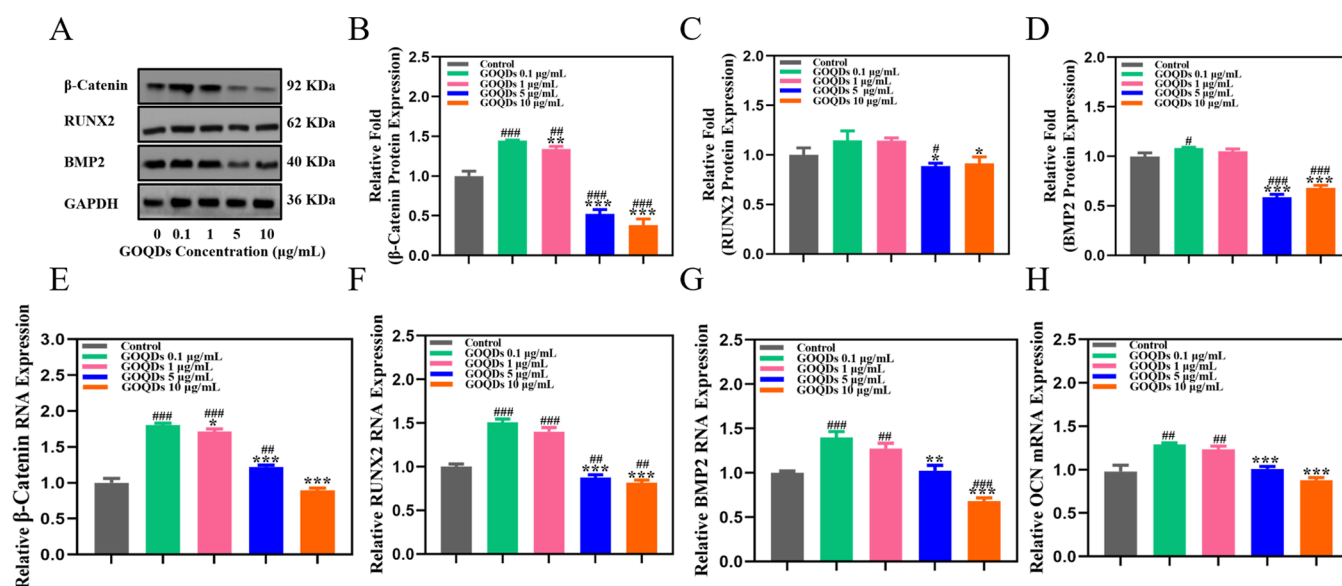


Figure 3. Western blotting and qRT-PCR analyses of the expression levels of osteogenic proteins and osteogenic genes after 7 days of incubation of BMSCs with GOQDs at different concentrations. (A) Expression levels of related proteins analyzed by western blotting; (B–D) quantitative analyses of β -catenin, Runt-related transcription factor 2 (RUNX2), and bone morphogenetic protein 2 (BMP2) protein expression; and (E–H) expression levels of osteogenic genes β -catenin, osteocalcin (OCN), BMP2, and RUNX2 in BMSCs tested by qRT-PCR (* p < 0.05, ** p < 0.01, and *** p < 0.001, compared with 0.1 μ g/mL GOQDs; # p < 0.05, ## p < 0.01, and ### p < 0.001, compared with control).

These studies reported that the proliferation of osteoblasts could be promoted when the concentration of graphene was lower than 10 μ g/mL. Therefore, in this study, a maximum of 10 μ g/mL was summarized as the low concentration for the experimental study. However, there are only a few reports on the study of different concentrations of GOQDs in terms of regulating the proliferation and differentiation of BMSCs.^{14,18} Some of these reports focused primarily on *in vitro* studies, and the mechanism has not been fully elucidated.

GO may regulate bone formation through some specific signaling pathways, such as Wnt/ β -catenin, PI3K/Akt/GSK-3 β / β -catenin, and MAPK signaling pathways.^{19–21} The Wnt/ β -catenin signaling pathway, as a classic signaling pathway in the process of bone formation, is a highly evolutionary conserved pathway that plays a vital role in bone regeneration.²² The promoting effects of graphene oxide nanoparticles on bone formation and regeneration may be related to the activation of the Wnt/ β -catenin signaling pathway.²³ β -catenin is an important sign of signaling pathway activation, which leads to the transcription of proteins in the Wnt/ β -catenin pathway and the activation of downstream target genes.²⁴

In the past, some scholars have studied the promotion of proliferation and differentiation of BMSCs by GO and its derivatives, with concentrations ranging from 0 to 50 μ g/mL or higher.^{17,23,25} However, other studies have reported that when the concentration of GO is greater than 10 μ g/mL, it will inhibit cell proliferation.¹⁸ Therefore, in this study, the upper concentration limit of 10 μ g/mL was selected, and the concentration of GOQDs was gradient-studied from 0 to 10 μ g/mL for analysis of the effects of GOQDs on the proliferation and differentiation of BMSCs in this low concentration range, which has rarely been reported in the literature. Our research team has made a preliminary exploration of the mechanism of graphene derivatives promoting bone formation and conducted *in vitro* experimental research.^{8,23} Based on our previous research, this study

systematically evaluated low-concentration nanoscale GOQDs. *In vitro* experiments were carried out at the same time, and preliminary exploration of *in vivo* experiments was conducted to provide new ideas and schemes for repairing bone tissue defects with nanomaterials. This study analyzed the effects of GOQDs at concentrations of 0, 0.1, 1, 5, and 10 μ g/mL on the proliferation and osteogenic differentiation of BMSCs *in vitro*. In addition, whether 0.1 μ g/mL GOQDs could promote bone defect repair *in vivo* was explored in this study. Further, the molecular mechanism of low concentrations of GOQDs to induce the osteogenic differentiation of BMSCs was preliminarily explored.

2. RESULTS

2.1. Characterization of GOQDs. In the Raman spectra of GOQDs (Figure 1B), the characteristic D band (\sim 1350 cm^{-1}) and G band (\sim 1580 cm^{-1}) of carbon materials can be observed.²⁶ The D band indicates the defect level and crystallinity of graphene, related to the sp^3 domain, while the G band indicates the vibration of sp^2 -bonded carbon atoms, related to the sp^2 structure. The morphology of GOQDs was observed by transmission electron microscopy (TEM, Hitachi, Japan). The lateral length of GOQDs was about 4–6 nm (Figure 1C).

2.2. Cell Viability, Cell Proliferation, and Cell Morphology. The survival numbers of BMSCs in different concentrations of GOQDs were measured by means of the Live/Dead viability kit. BMSCs were cocultured with GOQDs at concentrations of 0.1, 1, 5, and 10 μ g/mL for 3 days. Compared with the control group, when BMSCs were cocultured with GOQDs at concentrations of 0.1 and 1 μ g/mL, the survival rates of BMSCs increased significantly. In contrast, when BMSCs were cocultured with GOQDs at concentrations of 5 and 10 μ g/mL, their survival rate decreased (Figure 2A,B). After BMSCs were cocultured with different concentrations of GOQDs (0.1, 1, 5, and 10 μ g/mL) for 1 day, their proliferative ability was tested by the EdU

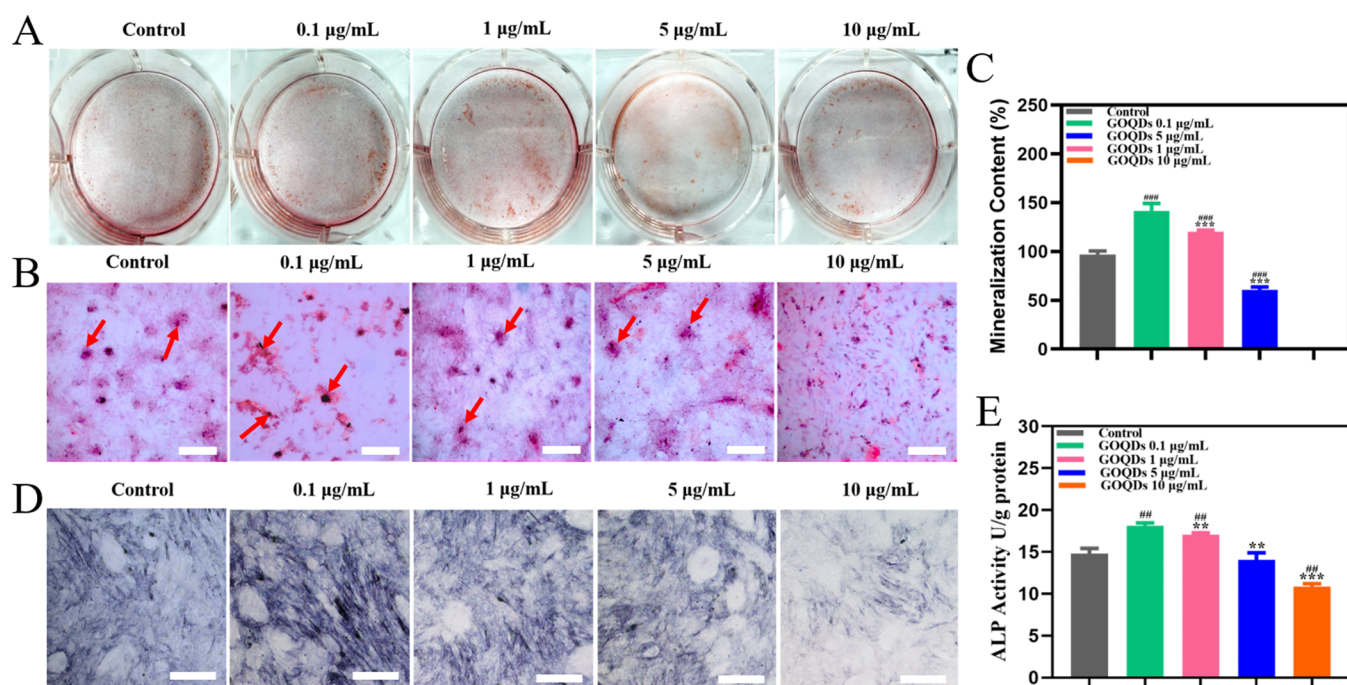


Figure 4. After BMSCs were cocultured with GOQDs at different concentrations, the effects of GOQDs on mineralization were detected. (A) Alizarin-red-stained image and (B) alizarin-red-stained calcium nodule image (represented by red arrows). Scale bars, 500 μm . (C) Semiquantitative detection of calcium nodules and (D) microscopic images of ALP staining. Scale bars, 200 μm . (E) Quantitative detection of ALP activity (* $p < 0.05$, *** $p < 0.01$, and **** $p < 0.001$, compared with 0.1 $\mu\text{g/mL}$ GOQDs; # $p < 0.05$, ## $p < 0.01$, and ### $p < 0.001$, compared with control).

proliferation assay. The experimental results (Figure 2C,D) showed that, compared with the untreated cell group, when BMSCs were cocultured with GOQDs at concentrations of 0.1 and 1 $\mu\text{g/mL}$, the ratio of EdU-positive cells in BMSCs increased significantly (2.17-fold and 1.72-fold, respectively, $p < 0.001$). In contrast, when BMSCs were treated with GOQDs at concentrations of 5 $\mu\text{g/mL}$ (0.82-fold, $p < 0.05$) and 10 $\mu\text{g/mL}$ (0.23-fold, $p < 0.001$), their proliferation rate decreased significantly. Compared with other groups, the number of BMSC nuclei treated with GOQDs at a concentration of 0.1 $\mu\text{g/mL}$ was the greatest (351 ± 15), while the number of nuclei treated with GOQDs at a concentration of 10 $\mu\text{g/mL}$ was the lowest (88 ± 4). In general, our results showed that low-dose GOQDs (0.1, 1 $\mu\text{g/mL}$), especially at a concentration of 0.1 $\mu\text{g/mL}$, had a beneficial effect on the growth of BMSCs, while high-dose GOQDs (5, 10 $\mu\text{g/mL}$) had an inhibitory effect on the proliferation of BMSCs.

2.3. Western Blotting and qRT-PCR. After BMSCs were cocultured with different concentrations of GOQDs (0.1, 1, 5, 10 $\mu\text{g/mL}$) for 7 days, western blotting and qRT-PCR were used to test the osteogenic protein expression levels and osteogenic gene expression levels in BMSCs. Western blotting analysis (Figure 3A–D) showed that, compared with the control group, on the 7th day of osteogenic differentiation, the expression levels of osteogenic protein increased significantly after BMSCs were cocultured with lower concentrations of GOQDs (0.1, 1 $\mu\text{g/mL}$). β -catenin protein expression levels (1.45-fold and 1.34-fold, respectively, $p < 0.01$) increased most significantly. In contrast, when BMSCs were cocultured with higher concentrations of GOQDs (5, 10 $\mu\text{g/mL}$), the osteogenic protein expression levels decreased significantly. The qRT-PCR results (Figure 3E–H) showed that, on the 7th day of osteogenic differentiation, as the concentrations of

GOQDs increased, the expression levels of osteogenic genes decreased. After low-concentration GOQDs (0.1, 1 $\mu\text{g/mL}$) were cocultured with BMSCs, the osteogenic gene expression levels of BMSCs were upregulated, while coculture with high-concentration GOQDs (5, 10 $\mu\text{g/mL}$) showed osteogenic gene expression to be downregulated compared with the control group. Overall, these results indicated that the low-concentration GOQDs (0.1, 1 $\mu\text{g/mL}$) enhanced the osteogenic differentiation of BMSCs, and that the optimal concentration of GOQDs that promoted the osteogenic differentiation of BMSCs was 0.1 $\mu\text{g/mL}$.

2.4. Alkaline Phosphatase (ALP) and Alizarin Red Staining. BMSCs were cocultured with different concentrations of GOQDs (0.1, 1, 5, 10 $\mu\text{g/mL}$) in an osteogenic medium for 14 days, and the calcium-rich deposits of osteoblast differentiation were analyzed by alizarin red staining. When BMSCs were cocultured with a lower concentration of GOQDs (0.1, 1 $\mu\text{g/mL}$), the numbers of calcium nodules increased, while coculture with higher concentrations of GOQDs (5, 10 $\mu\text{g/mL}$) showed that the numbers decreased (Figure 4B). The semiquantitative results of alizarin red staining (Figure 4C) indicated that, compared with the control group, the BMSCs cocultured with a low concentration of GOQDs (0.1, 1 $\mu\text{g/mL}$) were 142 and 120% higher, respectively. Both ALP staining and quantification were consistent with the alizarin red staining test. These findings further confirmed that low concentrations of GOQDs (0.1, 1 $\mu\text{g/mL}$) can promote the osteogenic differentiation of BMSCs.

2.5. Inhibitor Treatment. To explore the mechanism of osteogenic differentiation of BMSCs cocultured with GOQDs at a concentration of 0.1 $\mu\text{g/mL}$, we used western blotting to test the expression levels of proteins and genes related to the Wnt/ β -catenin signaling pathway. The expression levels of

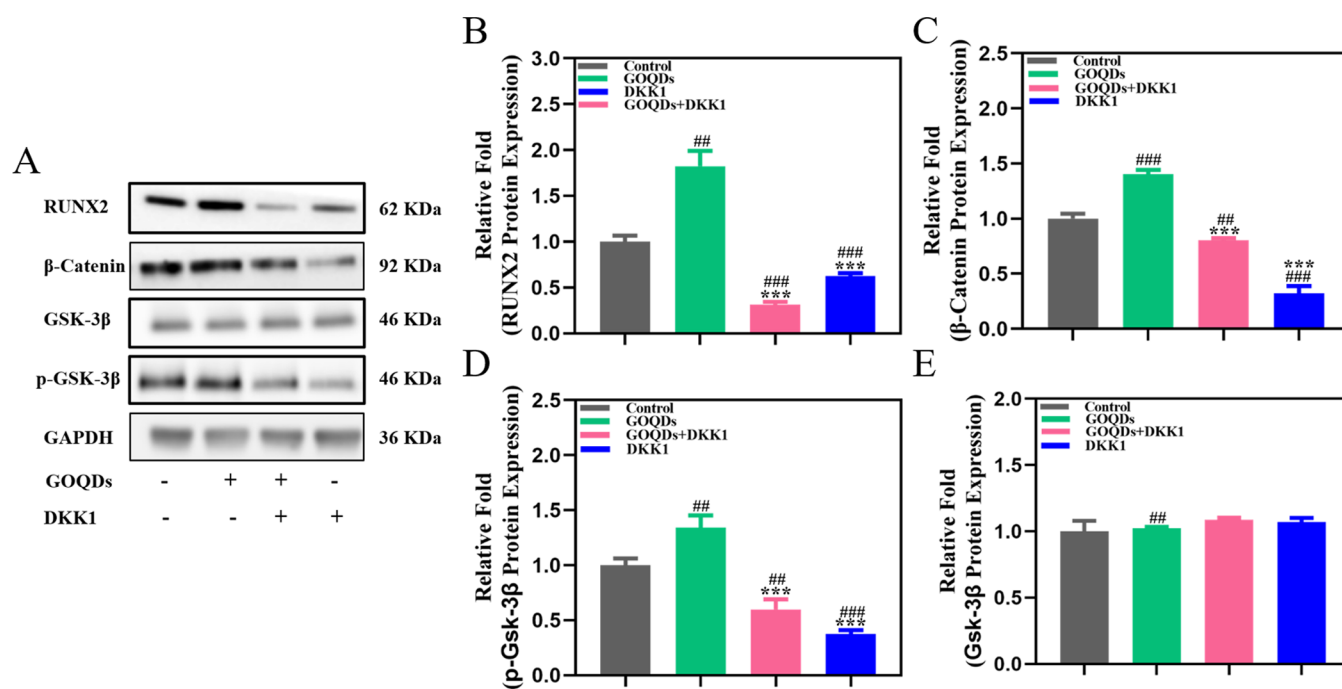


Figure 5. Western blotting was used to analyze the protein expression levels of RUNX2, β -catenin, p-GSK-3 β , and GSK-3 β of BMSCs cocultured with or without 0.1 μ g/mL GOQDs and DKK1 (an inhibitor of β -catenin). (A) Expression levels of related proteins tested by western blotting and (B–E) quantitative analysis of protein expression (* p < 0.05, ** p < 0.01, and *** p < 0.001, compared with 0.1 μ g/mL GOQDs; # p < 0.05, ## p < 0.01, and ### p < 0.001, compared with control).

total protein and phosphorylated protein of GSK-3 β (p-GSK-3 β) were detected. Compared with the control group, the p-GSK-3 β in BMSCs were significantly increased after GOQD treatment, while the total protein expression levels of GSK-3 β did not change significantly. The effects of GOQDs on β -catenin, p-GSK-3 β , and RUNX2 protein expression were significantly inhibited after cell treatment with Dickkopf-1-related protein 1 (DKK1). The results indicated that GOQDs activate the Wnt/ β -catenin signaling pathway (Figure 5).

For further verification of the role of the Wnt/ β -catenin pathway in GOQD-induced osteogenic differentiation of BMSCs, cells were pretreated with DKK1 (100 ng/mL) to inhibit the activation of the Wnt/ β -catenin signaling pathway. The qRT-PCR test results (Figure 6A–D) indicated that, after DKK1 treatment, the expression of osteogenic genes (BMP2, OCN, RUNX2, β -catenin) was significantly downregulated (0.73-fold, 0.75-fold, 0.69-fold, and 0.53-fold, respectively). Further, ALP activity and the degree of matrix mineralization were also significantly reduced (Figure 6E–I). These results further verified that GOQDs (0.1 μ g/mL) promote the osteogenic differentiation of BMSCs by activating the Wnt/ β -catenin signaling pathway.

2.6. Tissue Section Analysis. Energy dispersive spectrometry (EDS) was applied to determine the surface element types of Ti6Al4V scaffolds and sandblasted, large-grit, and acid-etched (SLA)-treated + GOQDs + Ti6Al4V scaffolds. As shown in Figure 7B,C, the spectra of the SLA-treated + GOQDs + Ti6Al4V scaffolds exhibited significant C and O peaks compared with those on the Ti6Al4V scaffolds, which were related to the successful coating of GOQDs on the SLA-treated Ti6Al4V scaffolds. The HE staining of superhard tissue sections (Figure 7D,E) showed that the three groups of Ti6Al4V scaffolds all had new bone formation after implantation, but that in the SAL + GOQD ($5.04 \pm 0.06\%$)

group was higher than those in the other two groups (control, $2.10 \pm 0.12\%$; SAL, $3.88 \pm 0.33\%$). Further, VG staining (Figure 7F,G) also showed that the three groups of Ti6Al4V scaffolds had new bone formation. The bone area proportion of SAL + GOQDs ($6.14 \pm 0.11\%$) was the greatest, which was statistically significantly different from that of the other two groups.

3. DISCUSSION

Graphene family materials have been widely studied in tissue engineering and nanomedicine. Recently developed GOQDs have further optimized their biocompatibility, cellular function, and anti-inflammatory properties, but their cytotoxicity cannot be eliminated.^{18,27} The concentrations of GOQDs are among the important factors affecting the proliferation and differentiation of BMSCs.¹⁷ Studies have reported that when nanomaterials are cocultured with cells, the changes in cell viability are closely related to the material dose.²⁸ Nanomaterials can trigger cellular stress responses or enhance therapeutic effects at lower doses.²⁹ In the low-dose/non-cytotoxic level range, heterogeneous cellular responses are a common feature of nanomaterial–biological interactions.³⁰ However, the effects of GOQD concentrations on BMSCs are rarely studied. In this study, we analyzed the effects of GOQDs of different concentrations on the proliferation and differentiation of BMSCs *in vivo* and *in vitro*. In addition, we also preliminarily explored whether low concentrations of GOQDs regulate the proliferation and differentiation of BMSCs by activating the Wnt/ β -catenin pathway.

The results of the Live/Dead cell-staining assay (Figure 2A,B) showed that GOQDs had dose-dependent toxicity to BMSCs. When the concentration of GOQDs was higher than 5 μ g/mL, the activity of BMSCs was inhibited compared with that of the control group. Similarly, the EdU proliferation test

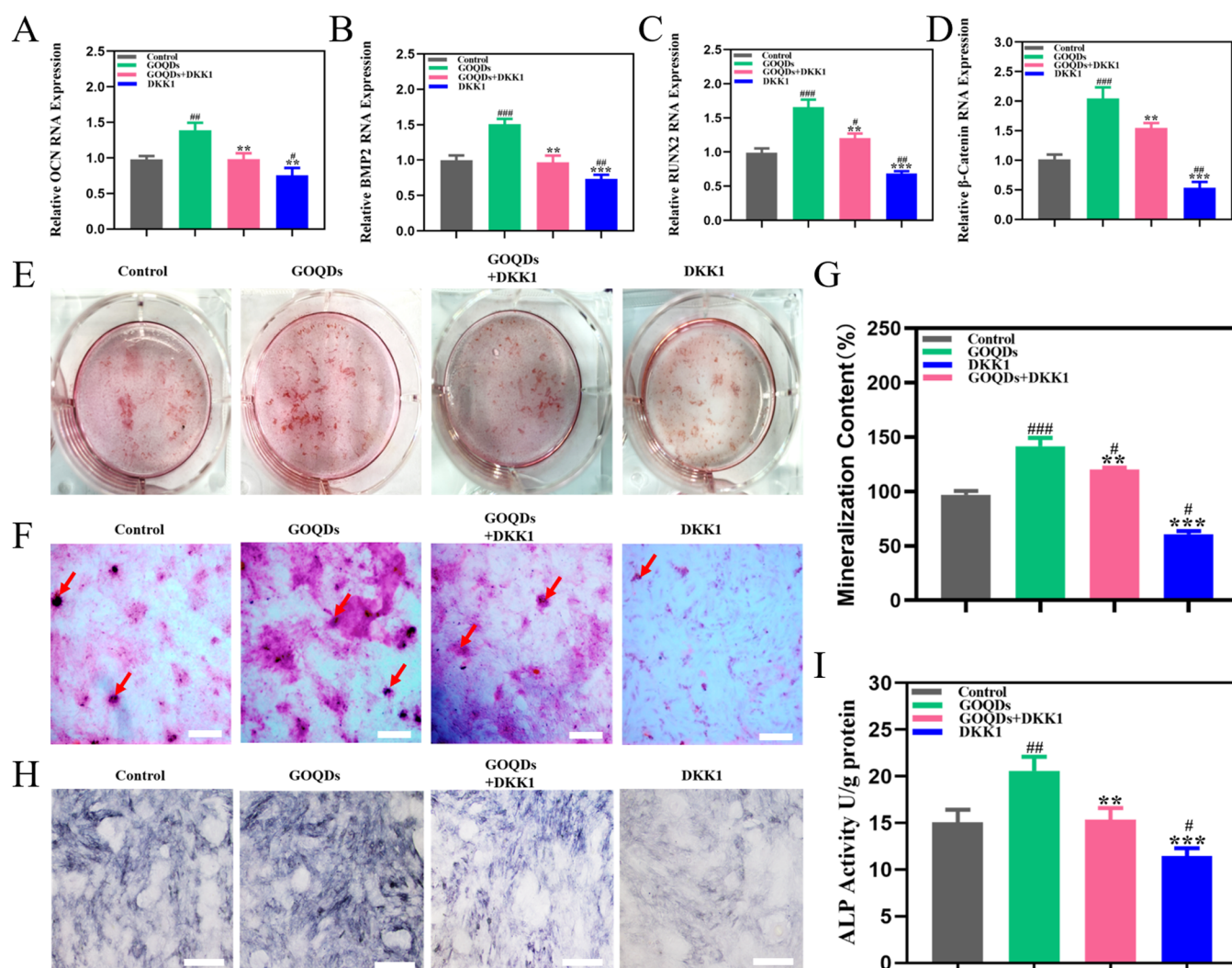


Figure 6. Effect of DKK1 on the osteogenic differentiation of BMSCs. (A–D) Osteogenic gene expressions of BMP2, OCN, β -catenin, and RUNX2 in BMSCs tested by qRT-PCR; (E) alizarin-red-stained image; (G) semiquantitative detection of calcium nodules; and (F) alizarin-red-stained calcium nodule image (represented by red arrows). Scale bars, 500 μ m. (H) Microscopic images of ALP staining. Scale bars, 200 μ m. (I) Quantitative detection of ALP activity (* p < 0.05, ** p < 0.01, and *** p < 0.001, compared with 0.1 μ g/mL GOQDs; # p < 0.05, ## p < 0.01, and ### p < 0.001, compared with control).

(Figure 2C,D) supported the previous conclusion. However, when the concentrations of GOQDs were 0.1 and 1 μ g/mL, GOQDs stimulated the proliferation and differentiation of BMSCs, and the optimal concentration of GOQDs for stimulating the proliferation and differentiation of BMSCs was 1 μ g/mL. After different concentrations of GOQDs stimulated BMSCs, their viability and proliferation ability were different because, at low concentrations, only a few cells were in contact with nanoparticles, and a relatively complete microenvironment remained. When the concentration of GOQDs increased gradually, the cytotoxicity increased, some cell structures were destroyed, and the number of cells decreased.¹⁷ Significant differences in cell viability have been reported after cells were treated with different concentrations of nanoparticles. When the concentrations of nanoparticles increased, nanoparticles aggregated and interacted with surrounding cells,^{31–33} which may lead to microenvironment granulation. Further, the adhesion of nanoparticles decreased and the risk of cell structure damage increased, resulting in inflammatory responses.^{33–35} Therefore, the principle of

microenvironment integrity can be used to explain the higher cell viability in GOQDs at 0.1 μ g/mL.

The results of cellular immunofluorescence staining (Figure 2E,F) showed that as the concentration of GOQDs increased, the numbers of actin filaments and cell nuclei gradually decreased. The high expression of actin stress fibers and the increase in the numbers of nuclei indicated that GOQDs (0.1 and 1 μ g/mL) had superior signal transduction in the process of osteogenic cell differentiation. When BMSCs were cocultured with GOQDs (5 and 10 μ g/mL), the numbers of nuclei decreased. It may be that these concentrations of GOQDs increased intracellular oxygen species (ROS) levels and superoxide dismutase (SOD) activity and decreased mitochondrial membrane potential.^{36,37}

Western blotting and qRT-PCR were used to detect the expression levels of osteogenesis-related proteins and genes. RUNX2 is a key regulator of osteogenic differentiation and osteogenic development, controlling the early stages of osteogenic development.^{38,39} β -catenin and BMP2 are important molecules involved in bone formation.⁴⁰ In addition, OCN plays an important role in bone formation and

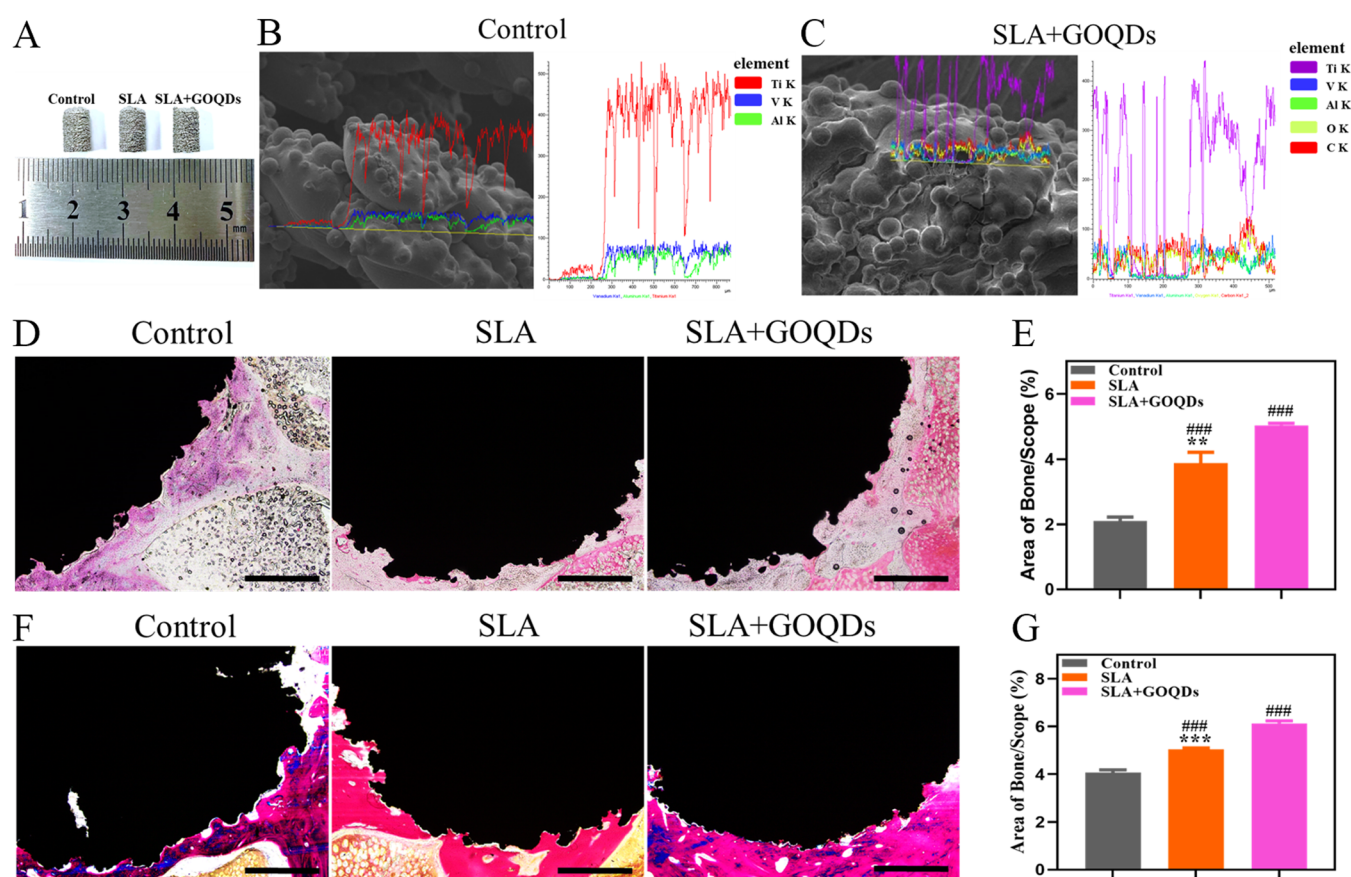


Figure 7. Histological analysis of new bone formation 3 months after scaffold implantation in rabbits. The new bone is red and the scaffold is black. (A) Physical image of the scaffold, (B) EDS of the Ti6Al4V scaffolds, (C) EDS of the SLA-treated + GOQDs + Ti6Al4V scaffolds, and (D) HE staining image of a superhard tissue section 3 months after the scaffold was implanted into the rabbit. The bone tissue is red and the Ti6Al4V scaffold is black. The light white or light red in the contact surface between the scaffold and the bone tissue is the new bone tissue. (E) Proportion of the new bone area on the scaffold after HE staining and (F) VG-stained image of a superhard tissue section 3 months after the scaffold was implanted into the rabbit. The bone tissue is red and the Ti6Al4V scaffold is black. The light white or light yellow in the contact surface between the scaffold and the bone tissue is the new bone tissue. (G) Proportion of new bone area on the scaffold after VG staining. Scale bars, 1000 μm (* $p < 0.05$, ** $p < 0.01$, and *** $p < 0.001$, compared with SLA + GOQDs; # $p < 0.05$, ## $p < 0.01$, and ### $p < 0.001$, compared with control).

remodeling.⁴¹ Therefore, RUNX2, β -catenin, BMP2, and OCN are key genes for the detection of bone formation. Western blotting and qRT-PCR results (Figure 3) indicated that the osteogenesis-related protein and gene expression levels decreased with increased GOQD concentrations. Compared with the other group, the osteogenic protein and osteogenic gene expression levels of GOQDs at 0.1 $\mu\text{g}/\text{mL}$ were the highest. In addition, this study found that, compared with other concentrations of GOQDs, GOQDs at 0.1 $\mu\text{g}/\text{mL}$ had a greater ability to increase the expression levels of β -catenin proteins and genes.

It is well known that ALP is an early marker of the osteogenic differentiation of BMSCs, and its activity reflects the degree of osteogenic differentiation.^{42,43} The ALP activity results (Figure 4D) showed that the ALP activity of GOQDs at 0.1 $\mu\text{g}/\text{mL}$ was higher than that of the control group. In addition, the content of calcium deposits in the extracellular matrix was detected by alizarin red staining (Figure 4A–C). Calcium deposits are considered to be a late marker of osteogenic differentiation. The results of alizarin red staining were consistent with those of the ALP activity test, indicating that GOQDs at 0.1 $\mu\text{g}/\text{mL}$ could improve the formation of calcium nodules.

The Wnt/ β -catenin signaling pathway plays an important role in regulating bone homeostasis. It can inhibit the differentiation of BMSCs into chondrocytes and adipocytes while improving the osteogenic differentiation of BMSCs.^{44–46} When the WNT signaling pathway is activated, the release of β -catenin in the cytoplasm increases, and β -catenin can be directly transferred to the nucleus to activate the transcription of downstream target genes. When GSK-3 β is active, β -catenin in the cytoplasm will be degraded by the complex (APC and Axin), so it cannot enter the nucleus smoothly. Conversely, when GSK-3 β loses its activity, β -catenin will not be degraded and enters the nucleus smoothly, thereby activating related signal molecules' downstream of the WNT signaling pathway and the transcription of downstream target genes.⁴⁷ Dkk1, as a secreted protein, can effectively inhibit WNT, with good specificity and high activity.⁴⁸ Studies have reported that Dkk1 binds to and isolates specific Frizzled receptors and low-density lipoprotein receptor-related protein 5 (LRP5) membrane complexes to inhibit the activity of WNT.⁴⁹ When the BMSCs were treated with 0.1 $\mu\text{g}/\text{mL}$ GOQDs, compared with the control group, the protein levels of p-GSK-3 β and β -catenin in BMSCs were upregulated and the protein levels of GSK-3 β remained unchanged (Figure 5). The ALP activity, osteogenic gene expression, and matrix mineralization of

BMSCs in 0.1 $\mu\text{g}/\text{mL}$ GOQDs were much higher than those in the control group. However, this promotion effect of 0.1 $\mu\text{g}/\text{mL}$ GOQDs can be specifically blocked by DKK1. The results indicated that 0.1 $\mu\text{g}/\text{mL}$ GOQDs may activate the Wnt/ β -catenin signaling pathway, improving the osteogenic differentiation of BMSCs. In addition, we also found that the expression of p-GSK-3 β and β -catenin protein and osteogenic gene expression of BMSCs in the 0.1 $\mu\text{g}/\text{mL}$ DKK1 + GOQDs group were higher than those in the DKK1 group. The ALP activity and the matrix mineralization degree of BMSCs in the 0.1 $\mu\text{g}/\text{mL}$ DKK1 + GOQDs group were still higher than those of the DKK1 group. These results indicated that 0.1 $\mu\text{g}/\text{mL}$ GOQDs can partially reverse the inhibitory effect of DKK1 by the Wnt/ β -catenin signaling pathway.

The results of HE and Masson staining (Figure 7) showed that new bone tissue formation was found at the interface between scaffolds and bone in the three groups, which was consistent with our previous research results, that is, that Ti6Al4V scaffolds have the ability to promote new bone formation.⁵⁰ However, the new bone area on SAL/GOQDs scaffolds was the greatest, which proved that GOQDs could accelerate bone tissue regeneration *in vivo*. In conclusion, low concentrations of GOQDs can promote the proliferation and differentiation of BMSCs *in vitro* and *in vivo*.

4. MATERIALS AND METHODS

4.1. Preparation and Characterization of Materials.

GOQD dispersions were provided from Nanjing Xianfeng (Nanjing XFNANO Materials, China) with a concentration of 1 mg/mL. The morphology and sizes of the GOQD particles obtained were detected by TEM. The number of layers and structural defects in GOQD nanosheets were detected by Raman spectroscopy (LabRAM HR Evolution, HORIBA).

4.2. BMSC Culture and Seeding. BMSCs were isolated from the femurs and tibiae of 4-week-old male Sprague-Dawley rats. Subsequently, BMSCs were seeded in DMEM-F12 containing 10% fetal bovine serum (FBS) and 1% penicillin–streptomycin and cultured in a humidified condition of 5% CO₂ at 37 °C. The culture medium was changed every 2–3 days. When the cell coverage reached 85–95% of the culture dish, the BMSCs were subcultured. In this study, all cells were used between generations 3 and 5.

4.3. Cell Viability and Cell Proliferation. Cell viability and cell proliferation were detected by means of the Live/Dead viability kit (calcein AM/PI, Bestbio, China) and the EdU proliferation kit (Beyotime, China), respectively. BMSCs were seeded in culture dishes at 5×10^4 cells per well, and then treated with GOQDs at different concentrations (0, 0.1, 1, 5, and 10 $\mu\text{g}/\text{mL}$). After 3 days of cell culture, the culture medium was removed, and cell viability was detected by means of the Live/Dead kit. After 1 day of cell culture, the culture medium was removed, and cell proliferation was detected by means of the EdU proliferation kit. The cell images were taken by laser confocal microscopy (Olympus, Japan).

4.4. Cell Morphology. The cell morphology of BMSCs treated with different concentrations of GOQDs was observed by laser confocal microscopy. BMSCs were seeded in culture dishes at 1×10^4 cells per well, and then treated with GOQDs of different concentrations (0, 0.1, 1, 5, and 10 $\mu\text{g}/\text{mL}$). After 3 days of BMSC culture, the culture medium was removed, and the BMSCs were fixed with 4% paraformaldehyde for 30 min at room temperature, and then infiltrated with 0.1% Triton X-100 for 15 min. A 100 μL quantity of phalloidin and 700 μL

of a DAPI solution (Solarbio, China) were used to stain the cells, and the cell images were taken by laser confocal microscopy.

4.5. ALP Staining and ALP Activity. ALP is an early marker for the detection of the osteogenic differentiation of BMSCs. BMSCs were seeded in a 24-well plate at a density of 2×10^4 cells per well and cultured with an osteogenic-inducing medium (OIM), then treated with GOQDs of different concentrations (0, 0.1, 1, 5, and 10 $\mu\text{g}/\text{mL}$). After 7 days of cell culture, ALP staining was detected by the BCIP/NBT ALP Color Development Kit (Beyotime, China) according to the manufacturer's protocol. For the testing of ALP activity, after 7 days of cell culture, protein concentrations were detected by the BCA protein test kit (Beyotime, China), and the ALP activity of BMSCs was detected by the ALP Kit (Nanjing Jiancheng, China).

4.6. Alizarin Red Staining. Alizarin red staining was used to evaluate the degree of matrix mineralization of BMSCs. BMSCs were seeded in a six-well plate at a density of 2×10^5 cells per well. After the BMSCs adhered to the wall, they were treated with different concentrations of GOQDs in OIM. After 7 days of culture, the BMSCs were fixed in 4% paraformaldehyde for 1 h and stained with alizarin red (Cyan Biosciences, China) at room temperature for 45 min. Calcium nodules were captured by color fluorescence microscopy (Zeiss, Germany). A cetylpyridine solution at 10% (Sigma, USA) was added to the six-well plate, and the OD values were detected at 562 nm.

4.7. qRT-PCR. Cell seeding was the same as described above. After 7 days of culture at different concentrations of GOQDs in OIM, total RNA was extracted with a Trizol reagent (Thermo Fisher, USA). The gene expression levels of OCN, BMP2, RUNX2, and β -catenin were detected. GAPDH was used as an internal reference. The gene primer design is shown in Table S1 in the Supporting Information.

4.8. Western Blotting. BMSC seeding and processing methods were the same as described above. BMSCs underwent lysis with RIPA, the protein concentration was detected, separated by 10% SDS-PAGE (CWBIO, China), and transferred to a poly(vinylidene fluoride) membrane (CWBIO, China), which was blocked with (TBS + Tween) TBST containing 5% skimmed milk at room temperature for 60 min, incubated with primary antibodies against RUNX2, β -catenin, OCN, BMP2, GSK-3 β , p-GSK-3 β , and GAPDH at 4 °C overnight. The membranes were washed in TBST and incubated with the secondary antibody for 2 h at room temperature.

4.9. Inhibitor Treatment. BMSCs were treated with or without GOQDs at a concentration of 0.1 $\mu\text{g}/\text{mL}$. When the cell coverage area reached 70% of the culture dish, DKK1 was added or not for cell treatment. The cells were divided into four groups: a control group (BMSCs cultured in OIM alone), the DKK1 group (BMSCs cultured in OIM and DKK1), the DKK1 + GOQD group (BMSCs cultured in OIM, DKK1, and GOQDs), and the GOQD group (BMSCs cultured in OIM and GOQDs). The expression levels of osteogenic genes and proteins were detected by qRT-PCR and western blotting.

4.10. Animal Model. Ti6Al4V scaffolds with a diameter of 5 mm and a height of 8 mm were provided by the Metal Research Institute, Chinese Academy of Sciences (Shenyang, China). According to the methods of previous research, SLA scaffold surfaces were obtained by etching the scaffolds in the mixed liquids of HCl and H₂SO₄ in a 60 °C bain-marie

(double boiler) for 8 h.⁵¹ Then, SLA-treated scaffolds were soaked in the GOQDs at a concentration of 0.1 $\mu\text{g}/\text{mL}$ and placed on the shaking table of a 4 °C chromatography cabinet for 24 h. After scaffolds were freeze-dried, the functionalized modified titanium surfaces were obtained and stored at 4 °C. The elemental compositions of Ti6Al4V scaffolds and SLA-treated + GOQDs + Ti6Al4V scaffolds were analyzed by EDS.

All animal experiments were conducted in accordance with the principles and procedures approved by the Experimental Animal Ethics Committee of Sun Yat-sen University (Approval number: SYSUIACUC-2019-000169). A total of 18 adult male New Zealand white rabbits (2.5–3.0 kg) were randomly divided into three groups: the Ti6Al4V scaffold group (control group), the SLA-treated Ti6Al4V scaffold group (SLA group), and the SLA-treated + GOQDs + Ti6Al4V scaffold group (SLA + GOQDs group). The three groups of scaffolds were implanted into the rabbits' femurs, and bone tissue regeneration was analyzed after 3 months.

4.11. Histological Analysis. All samples were gradually dehydrated in 70, 80, and 90% *n*-butanol and absolute ethanol, embedded, and the tissue was cut into 60- μm -thick sections by means of a superhard tissue slicer and subjected to HE and VG staining. The bone tissue regeneration of the scaffolds was observed by fluorescence microscopy (Olympus, Japan).

4.12. Statistical Analysis. All quantitative results in this study are given as mean \pm standard deviation (SD). The significant differences between and among groups were evaluated by *t*-test and one-way analysis of variance (ANOVA). *p* < 0.05 was considered a significant difference.

5. CONCLUSIONS

This study explored the effects of different concentrations of GOQDs on the osteogenic differentiation of BMSCs and initially explored the molecular mechanism of GOQDs for improving the osteogenic differentiation of BMSCs. GOQDs with concentrations lower than 1 $\mu\text{g}/\text{mL}$ significantly improved the activity and proliferation ability of BMSCs. Compared with other concentrations, GOQDs at a concentration of 0.1 $\mu\text{g}/\text{mL}$ significantly promoted the osteogenic differentiation of BMSCs. Therefore, in this study, the optimal concentration of GOQDs to promote the proliferation and differentiation of BMSCs was 0.1 $\mu\text{g}/\text{mL}$. In addition, this study also demonstrated that GOQDs at a concentration of 0.1 $\mu\text{g}/\text{mL}$ activated the Wnt/ β -catenin signaling pathway to promote the osteogenic differentiation of BMSCs. Furthermore, the GOQDs with a concentration of 0.1 $\mu\text{g}/\text{mL}$, modified on the surfaces of Ti6Al4V scaffolds, accelerated the formation of new bones. These findings provide a theoretical basis for GOQDs to regulate the osteogenic differentiation of BMSCs to repair bone defects.

■ ASSOCIATED CONTENT

SI Supporting Information

The Supporting Information is available free of charge at <https://pubs.acs.org/doi/10.1021/acsomega.1c06892>.

Gene expression levels of OCN, BMP2, RUNX2, and β -catenin were detected, GAPDH was used as an internal reference, and gene primer design is shown in Table S1 (PDF)

■ AUTHOR INFORMATION

Corresponding Authors

Dongsheng Yu – Hospital of Stomatology, Sun Yat-sen University, Guangzhou, Guangdong 510055, P. R. China; Guangdong Provincial Key Laboratory of Stomatology, Sun Yat-sen University, Guangzhou, Guangdong 510050, P. R. China; orcid.org/0000-0002-2176-9308; Email: yudsh@mail.sysu.edu.cn

Wei Zhao – Hospital of Stomatology, Sun Yat-sen University, Guangzhou, Guangdong 510055, P. R. China; Guangdong Provincial Key Laboratory of Stomatology, Sun Yat-sen University, Guangzhou, Guangdong 510050, P. R. China; Email: zhaowei3@mail.sysu.edu.cn

Authors

Duoling Xu – Hospital of Stomatology, Sun Yat-sen University, Guangzhou, Guangdong 510055, P. R. China; Guangdong Provincial Key Laboratory of Stomatology, Sun Yat-sen University, Guangzhou, Guangdong 510050, P. R. China; orcid.org/0000-0003-1657-8723

Chao Wang – Hospital of Stomatology, Sun Yat-sen University, Guangzhou, Guangdong 510055, P. R. China; Guangdong Provincial Key Laboratory of Stomatology, Sun Yat-sen University, Guangzhou, Guangdong 510050, P. R. China; orcid.org/0000-0001-8384-0977

Jie Wu – Hospital of Stomatology, Sun Yat-sen University, Guangzhou, Guangdong 510055, P. R. China; Guangdong Provincial Key Laboratory of Stomatology, Sun Yat-sen University, Guangzhou, Guangdong 510050, P. R. China

Yuanxiang Fu – School of Chemical Engineering & Guizhou Provincial Key Laboratory of Energy Chemistry, Guizhou Institute of Technology, Guiyang 550003, P. R. China

Shujun Li – Institute of Metal Research, Chinese Academy of Sciences, Shenyang, Liaoning 110016, P. R. China

Wentao Hou – Institute of Metal Research, Chinese Academy of Sciences, Shenyang, Liaoning 110016, P. R. China

Ling Lin – Hospital of Stomatology, Sun Yat-sen University, Guangzhou, Guangdong 510055, P. R. China; Guangdong Provincial Key Laboratory of Stomatology, Sun Yat-sen University, Guangzhou, Guangdong 510050, P. R. China

Pei Li – Hospital of Stomatology, Sun Yat-sen University, Guangzhou, Guangdong 510055, P. R. China; Guangdong Provincial Key Laboratory of Stomatology, Sun Yat-sen University, Guangzhou, Guangdong 510050, P. R. China

Complete contact information is available at:

<https://pubs.acs.org/doi/10.1021/acsomega.1c06892>

Author Contributions

[†]D.X. and C.W. equally contributed to this work. All authors have given approval to the final version of the manuscript.

Notes

The authors declare no competing financial interest.

■ ACKNOWLEDGMENTS

This work was financially supported by the National Natural Science Foundation of China (Nos. 81974146, 81873711), the Science and Technology Planning Project of Guangdong Province (2016A020215094), and the Special Funds for the Cultivation of Guangdong College Students' Scientific and Technological Innovation ("Climbing Program" Special Funds, pdjh 2022b0012).

REFERENCES

- (1) Yang, J.; Qin, H. J.; Chai, Y.; Zhang, P.; Chen, Y. R.; Yang, K.; Qin, M.; Zhang, Y. F.; Xia, H.; Ren, L.; Yu, B. Molecular mechanisms of osteogenesis and antibacterial activity of Cu-bearing Ti alloy in a bone defect model with infection in vivo. *J Orthop Transl* **2021**, *27*, 77–89.
- (2) Lin, J.; Chen, L.; Dou, D. Progress of orthopaedic research in China over the last decade. *J Orthop Transl* **2020**, *24*, 131–137.
- (3) Choi, S.; Jo, H. S.; Song, H.; Kim, H. J.; Oh, J. K.; Cho, J. W.; Park, K.; Kim, S. E. Multifunctional Tannic Acid-Alendronate Nanocomplexes with Antioxidant, Anti-Inflammatory, and Osteogenic Potency. *Nanomaterials-Basel* **2021**, *11*, 1812.
- (4) Toda, E.; Bai, Y. P.; Sha, J. J.; Dong, Q. N.; Ngo, H. X.; Suyama, T.; Miyamoto, K.; Matsuzaki, Y.; Kanno, T. Feasibility of Application of the Newly Developed Nano-Biomaterial, beta-TCP/PDLLA, in Maxillofacial Reconstructive Surgery: A Pilot Rat Study. *Nanomaterials-Basel* **2021**, *11*, 303.
- (5) Yang, A. F.; Yu, C. C.; Lu, Q. L.; Li, H.; Li, Z. H.; He, C. J. Mechanism of Action of Icarin in Bone Marrow Mesenchymal Stem Cells. *Stem Cells Int* **2019**, *2019*, No. 5747298.
- (6) Panetta, N. J.; Gupta, D. M.; Longaker, M. T. Bone Regeneration and Repair. *Curr. Stem. Cell Res. Ther.* **2010**, *5*, 122–128.
- (7) Pittenger, M. F.; Mackay, A. M.; Beck, S. C.; Jaiswal, R. K.; Douglas, R.; Mosca, J. D.; Moorman, M. A.; Simonetti, D. W.; Craig, S.; Marshak, D. R. Multilineage potential of adult human mesenchymal stem cells. *Science* **1999**, *284*, 143–147.
- (8) Grant, J. J.; Pillai, S. C.; Hehir, S.; McAfee, M.; Breen, A. Biomedical Applications of Electrospun Graphene Oxide. *ACS Biomater. Sci. Eng.* **2021**, *7*, 1278–1301.
- (9) Adil, S. F.; Shaik, M. R.; Nasr, F. A.; Alqahtani, A. S.; Ahmed, M. Z.; Qamar, W.; Kuniyil, M.; Almutairi, A.; Alwarthan, A.; Siddiqui, M. R. H.; Hatshan, M. R.; Khan, M. Enhanced Apoptosis by Functionalized Highly Reduced Graphene Oxide and Gold Nanocomposites in MCF-7 Breast Cancer Cells. *ACS Omega* **2021**, *6*, 15147–15155.
- (10) Turk, M.; Deliormanli, A. M. Electrically conductive borate-based bioactive glass scaffolds for bone tissue engineering applications. *J. Biomater. Appl.* **2017**, *32*, 28–39.
- (11) Li, P. L.; Di Stasio, F.; Eda, G.; Fenwick, O.; McDonnell, S. O.; Anderson, H. L.; Chhowalla, M.; Cacialli, F. Luminescent Properties of a Water-Soluble Conjugated Polymer Incorporating Graphene-Oxide Quantum Dots. *ChemPhysChem* **2015**, *16*, 1258–1262.
- (12) Ko, N. R.; Nafiujjaman, M.; Lee, J. S.; Lim, H. N.; Lee, Y. K.; Kwon, I. K. Graphene quantum dot-based theranostic agents for active targeting of breast cancer. *RSC Adv.* **2017**, *7*, 11420–11427.
- (13) Tabish, T. A.; Scotton, C. J.; Ferguson, D. C. J.; Lin, L. X.; van der Veen, A.; Lowry, S.; Ali, M.; Jabeen, F.; Winyard, P. G.; Zhang, S. W. Biocompatibility and toxicity of graphene quantum dots for potential application in photodynamic therapy. *Nanomedicine* **2018**, *13*, 1923–1937.
- (14) Zhang, X. L.; Wei, C. B.; Li, Y. M.; Li, Y.; Chen, G. H.; He, Y.; Yi, C.; Wang, C.; Yu, D. S. Dose-dependent cytotoxicity induced by pristine graphene oxide nanosheets for potential bone tissue regeneration. *J. Biomed. Mater. Res., Part A* **2020**, *108*, 614–624.
- (15) Qiao, K.; Guo, S. L.; Zheng, Y. D.; Xu, X. T.; Meng, H. Y.; Peng, J.; Fang, Z. Y.; Xie, Y. J. Effects of graphene on the structure, properties, electro-response behaviors of GO/PAA composite hydrogels and influence of electro-mechanical coupling on BMSC differentiation. *Mater. Sci. Eng., C* **2018**, *93*, 853–863.
- (16) Wang, X. T.; Guo, W. M.; Li, L. Y.; Yu, F.; Li, J. Y.; Liu, L.; Fang, B.; Xia, L. G. Photothermally triggered biomimetic drug delivery of Teriparatide via reduced graphene oxide loaded chitosan hydrogel for osteoporotic bone regeneration. *Chem. Eng. J.* **2021**, *413*, No. 127413.
- (17) Liao, T. T.; Deng, Q. Y.; Wu, B. J.; Li, S. S.; Li, X.; Wu, J.; Leng, Y. X.; Guo, Y. B.; Huang, N. Dose-dependent cytotoxicity evaluation of graphite nanoparticles for diamond-like carbon film application on artificial joints. *Biomed. Mater.* **2017**, *12*, No. 015018.
- (18) Qiu, J. C.; Li, D. S.; Mou, X. N.; Li, J. H.; Guo, W. B.; Wang, S.; Yu, X.; Ma, B. J.; Zhang, S.; Tang, W.; Sang, Y. H.; Gil, P. R.; Liu, H. Effects of Graphene Quantum Dots on the Self-Renewal and Differentiation of Mesenchymal Stem Cells. *Adv. Healthcare Mater.* **2016**, *5*, 702–710.
- (19) Wu, C. T.; Xia, L. G.; Han, P. P.; Xu, M. C.; Fang, B.; Wang, J. C.; Chang, J.; Xiao, Y. Graphene-oxide-modified beta-tricalcium phosphate bioceramics stimulate in vitro and in vivo osteogenesis. *Carbon* **2015**, *93*, 116–129.
- (20) Wu, X. W.; Zheng, S.; Ye, Y. Z.; Wu, Y. C.; Lin, K. L.; Su, J. S. Enhanced osteogenic differentiation and bone regeneration of poly(lactic-co-glycolic acid) by graphene via activation of PI3K/Akt/GSK-3 beta-beta-catenin signal circuit. *Biomater. Sci.* **2018**, *6*, 1147–1158.
- (21) Chen, Y. H.; Zheng, Z. W.; Zhou, R. P.; Zhang, H. Z.; Chen, C. S.; Xiong, Z. Z.; Liu, K.; Wang, X. S. Developing a Strontium-Releasing Graphene Oxide-/Collagen-Based Organic Inorganic Nanobiocomposite for Large Bone Defect Regeneration via MAPK Signaling Pathway. *ACS Appl. Mater. Interfaces* **2019**, *11*, 15986–15997.
- (22) Yao, Q.; Yu, C.; Zhang, X.; Zhang, K.; Guo, J.; Song, L. Wnt/beta-catenin signaling in osteoblasts regulates global energy metabolism. *Bone* **2017**, *97*, 175–183.
- (23) He, Y.; Li, Y. M.; Chen, G. H.; Wei, C. B.; Zhang, X. L.; Zeng, B. H.; Yi, C.; Wang, C.; Yu, D. S. Concentration-dependent cellular behavior and osteogenic differentiation effect induced in bone marrow mesenchymal stem cells treated with magnetic graphene oxide. *J. Biomed. Mater. Res., Part A* **2020**, *108*, 50–60.
- (24) Reya, T.; Clevers, H. Wnt signalling in stem cells and cancer. *Nature* **2005**, *434*, 843–850.
- (25) Yang, X.; Zhao, Q.; Chen, Y. J.; Fu, Y. X.; Lu, S. S.; Yu, X. L.; Yu, D. S.; Zhao, W. Effects of graphene oxide and graphene oxide quantum dots on the osteogenic differentiation of stem cells from human exfoliated deciduous teeth. *Artif. Cells, Nanomed., Biotechnol.* **2019**, *47*, 822–832.
- (26) Zhu, Y.; Cao, H. L.; Qiao, S. C.; Wang, M. L.; Gu, Y. X.; Luo, H. W.; Meng, F. H.; Liu, X. Y.; Lai, H. C. Hierarchical micro/nanostructured titanium with balanced actions to bacterial and mammalian cells for dental implants. *Int. J. Nanomed.* **2015**, *10*, 6659–6674.
- (27) Ferrari, A. C.; Robertson, J. Interpretation of Raman spectra of disordered and amorphous carbon. *Phys. Rev. B* **2000**, *61*, 14095–14107.
- (28) Jia, H. N.; Cai, Y. F.; Lin, J. H.; Liang, H. Y.; Qi, J. L.; Cao, J.; Feng, J. C.; Fei, W. D. Heterostructural Graphene Quantum Dot/MnO₂ Nanosheets toward High-Potential Window Electrodes for High-Performance Supercapacitors. *Adv. Sci.* **2018**, *5*, No. 1700887.
- (29) Wu, Z. R.; Shi, P. J.; Lim, H. K.; Ma, Y. Y.; Setyawati, M. I.; Bitounis, D.; Demokritou, P.; Ng, K. W.; Tay, C. Y. Inflammation Increases Susceptibility of Human Small Airway Epithelial Cells to Pneumonic Nanotoxicity. *Small* **2020**, *16*, No. 2000963.
- (30) Bell, I. R.; Ives, J. A.; Jonas, W. B. Nonlinear Effects of Nanoparticles: Biological Variability from Hormetic Doses, Small Particle Sizes, and Dynamic Adaptive Interactions. *Dose-Response* **2014**, *12*, 202–232.
- (31) Wu, Z. R.; Yang, H. B.; Archana, G.; Rakshit, M.; Ng, K. W.; Tay, C. Y. Human keratinocytes adapt to ZnO nanoparticles induced toxicity via complex paracrine crosstalk and Nrf2-proteasomal signal transduction. *Nanotoxicology* **2018**, *12*, 1215–1229.
- (32) Fröhlich, E.; Meindl, C.; Roblegg, E.; Griesbacher, A.; Pieber, T. R. Cytotoxicity of nanoparticles is influenced by size, proliferation and embryonic origin of the cells used for testing. *Nanotoxicology* **2012**, *6*, 424–439.
- (33) Ajita, J.; Saravanan, S.; Selvamurugan, N. Effect of size of bioactive glass nanoparticles on mesenchymal stem cell proliferation for dental and orthopedic applications. *Mater. Sci. Eng., C* **2015**, *53*, 142–149.
- (34) Yang, L.; Yan, Q. Q.; Zhao, J.; Li, J.; Zong, X. C.; Yang, L.; Wang, Z. L. The role of potassium channel in silica nanoparticle-

induced inflammatory effect in human vascular endothelial cells in vitro. *Toxicol. Lett.* **2013**, *223*, 16–24.

(35) Olteanu, D.; Filip, A.; Socaci, C.; Biris, A. R.; Filip, X.; Coros, M.; Rosu, M. C.; Pogacean, F.; Alb, C.; Baldea, I.; Bolfa, P.; Pruneanu, S. Cytotoxicity assessment of graphene-based nanomaterials on human dental follicle stem cells. *Colloids Surf, B* **2015**, *136*, 791–798.

(36) Talukdar, Y.; Rashkow, J. T.; Lalwani, G.; Kanakia, S.; Sitharaman, B. The effects of graphene nanostructures on mesenchymal stem cells. *Biomaterials* **2014**, *35*, 4863–4877.

(37) Besseling, E.; Wang, B.; Lurling, M.; Koelmans, A. A. Nanoplastic Affects Growth of *S. obliquus* and Reproduction of *D. magna*. *Environ. Sci. Technol.* **2014**, *48*, 12336–12343.

(38) Perreault, F.; Samadani, M.; Dewez, D. Effect of soluble copper released from copper oxide nanoparticles solubilisation on growth and photosynthetic processes of *Lemna gibba* L. *Nanotoxicology* **2014**, *8*, 374–382.

(39) Narayanan, A.; Srinaath, N.; Rohini, M.; Selvamurugan, N. Regulation of Runx2 by MicroRNAs in osteoblast differentiation. *Life Sci.* **2019**, *232*, No. 116676.

(40) Stein, G. S.; Lian, J. B.; van Wijnen, A. J.; Stein, J. L.; Montecino, M.; Javed, A.; Zaidi, S. K.; Young, D. W.; Choi, J. Y.; Pockwinse, S. M. Runx2 control of organization, assembly and activity of the regulatory machinery for skeletal gene expression. *Oncogene* **2004**, *23*, 4315–4329.

(41) Karoulias, S. Z.; Pitou, M.; Papi, R.; Lamprou, P.; Choli-Papadopoulou, T. Specific amino acids from the broad C-terminal region of BMP-2 are crucial for osteogenesis. *Bone Rep.* **2021**, *14*, No. 101092.

(42) Wang, G. C.; Zheng, L.; Zhao, H. S.; Miao, J. Y.; Sun, C. H.; Ren, N.; Wang, J. Y.; Liu, H.; Tao, X. T. In Vitro Assessment of the Differentiation Potential of Bone Marrow-Derived Mesenchymal Stem Cells on Genipin-Chitosan Conjugation Scaffold with Surface Hydroxyapatite Nanostructure for Bone Tissue Engineering. *Tissue Eng., Part A* **2011**, *17*, 1341–1349.

(43) Yang, Y.; Xu, T.; Zhang, Q.; Piao, Y.; Bei, H. P.; Zhao, X. Biomimetic, Stiff, and Adhesive Periosteum with Osteogenic-Angiogenic Coupling Effect for Bone Regeneration. *Small* **2021**, *17*, No. e2006598.

(44) Yang, Y. H.; Zhang, Q.; Xu, T. P.; Zhang, H. Y.; Zhang, M.; Lu, L.; Hao, Y. F.; Fuh, J. Y. H.; Zhao, X. Photocrosslinkable nanocomposite ink for printing strong, biodegradable and bioactive bone graft. *Biomaterials* **2020**, *263*, No. 120378.

(45) Bullock, W. A.; Robling, A. G. WNT-mediated Modulation of Bone Metabolism: Implications for WNT Targeting to Treat Extraskelletal Disorders. *Toxicol. Pathol.* **2017**, *45*, 864–868.

(46) Li, Y.; Jin, D. X.; Xie, W. X.; Wen, L. F.; Chen, W. J.; Xu, J. X.; Ding, J. Y.; Ren, D. C. PPAR-gamma and Wnt Regulate the Differentiation of MSCs into Adipocytes and Osteoblasts Respectively. *Curr. Stem. Cell Res. Ther.* **2018**, *13*, 185–192.

(47) Li, R.; Xu, J. B.; Wong, D. S. H.; Li, J. M.; Zhao, P. C.; Bian, L. M. Self-assembled N-cadherin mimetic peptide hydrogels promote the chondrogenesis of mesenchymal stem cells through inhibition of canonical Wnt/beta-catenin signaling. *Biomaterials* **2017**, *145*, 33–43.

(48) MacDonald, B. T.; Tamai, K.; He, X. Wnt/beta-Catenin Signaling: Components, Mechanisms, and Diseases. *Dev. Cell* **2009**, *17*, 9–26.

(49) Pinzone, J. J.; Hall, B. M.; Thudi, N. K.; Vonau, M.; Qiang, Y. W.; Rosol, T. J.; Shaughnessy, J. D. The role of Dickkopf-1 in bone development, homeostasis, and disease. *Blood* **2009**, *113*, 517–525.

(50) Glantschnig, H.; Hampton, R. A.; Lu, P.; Zhao, J. Z.; Vitelli, S.; Huang, L. Y.; Haytko, P.; Cusick, T.; Ireland, C.; Jarantow, S. W.; Ernst, R.; Wei, N.; Nantermet, P.; Scott, K. R.; Fisher, J. E.; Talamo, F.; Orsatti, L.; Reszka, A. A.; Sandhu, P.; Kimmel, D.; Flores, O.; Strohl, W.; An, Z. Q.; Wang, F. B. Generation and Selection of Novel Fully Human Monoclonal Antibodies That Neutralize Dickkopf-1 (DKK1) Inhibitory Function in Vitro and Increase Bone Mass in Vivo. *J. Biol. Chem.* **2010**, *285*, 40135–40147.

(51) Wang, C.; Xu, D. L.; Lin, L.; Li, S. J.; Hou, W. T.; He, Y.; Sheng, L. Y.; Yi, C.; Zhang, X. L.; Li, H. Y.; Li, Y. M.; Zhao, W.; Yu,

D. S. Large-pore-size Ti6Al4V scaffolds with different pore structures for vascularized bone regeneration. *Mater. Sci. Eng., C* **2021**, *131*, No. 112499.